Supporting Information

Stacking Up Layers of Polyaniline/Carbon Nanotube Network Inside Papers as Highly Flexible Electrodes with Large Areal Capacitance and Superior Rate Capability

Liubing Dong [a,b], Gemeng Liang [a], Chengjun Xu [a,*], Danyang Ren [a], Jinjie Wang [a], Zheng-Ze Pan [a], Baohua Li [a], Feiyu Kang [a,b*], Quan-Hong Yang [a,c]

[a] Graduate School at Shenzhen, Tsinghua University, Shenzhen 518055, China

[b] State Key Laboratory of New Ceramics and Fine Processing, School of Materials Science and Engineering, Tsinghua University, Beijing 100084, China

[c] School of Chemical Engineering and Technology, Tianjin University, Tianjin 300072, China

*Corresponding authors and email address：

vivaxuchengjun@163.com (C. Xu); fykang@mail.tsinghua.edu.cn (F. Kang)

Experimental section: Calculation methods for gravimetric capacitance of PANI in PANI/CNT/paper electrodes

(1) For A(2C*y*P)1 composite paper electrodes, gravimetric capacitance of PANI ($C_{m,PANI1}$, F g^{-1}) was calculated according to *Equation* (S1),

$$C_{m,PANI1} = \frac{C_{s,A(2CyP)1} - C_{s,A(2C)1}}{m_{PANI1}} \quad \text{(S1)}$$

where $C_{s,A(2CyP)1}$ (mF cm^{-2}) and $C_{s,A(2C)1}$ (mF cm^{-2}) were areal capacitances of A(2C*y*P)1 and A(2C)1 paper electrodes, respectively, and m_{PANI1} (mg cm^{-2}) was mass of PANI in A(2C*y*P)1.

(2) For A(2C0.5P)*n* composite paper electrodes, gravimetric capacitance of PANI ($C_{m,PANI2}$, F g^{-1}) was calculated according to *Equation* (S2),

$$C_{m,PANI2} = \frac{C_{s,A(2C0.5P)n} - C_{s,A(2C)n}}{m_{PANI2}} \quad \text{(S2)}$$

where $C_{s,A(2C0.5P)n}$ (mF cm^{-2}) and $C_{s,A(2C)n}$ (mF cm^{-2}) were areal capacitances of A(2C0.5P)*n* and A(2C)*n* paper electrodes, respectively, and m_{PANI2} (mg cm^{-2}) was mass of PANI in A(2C0.5P)*n*.

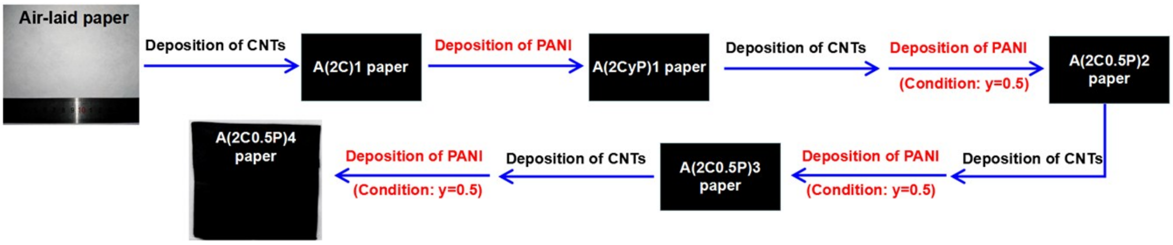

Fig. S1 Schematic of stacking up layers of PANI/CNT network inside an air-laid paper.

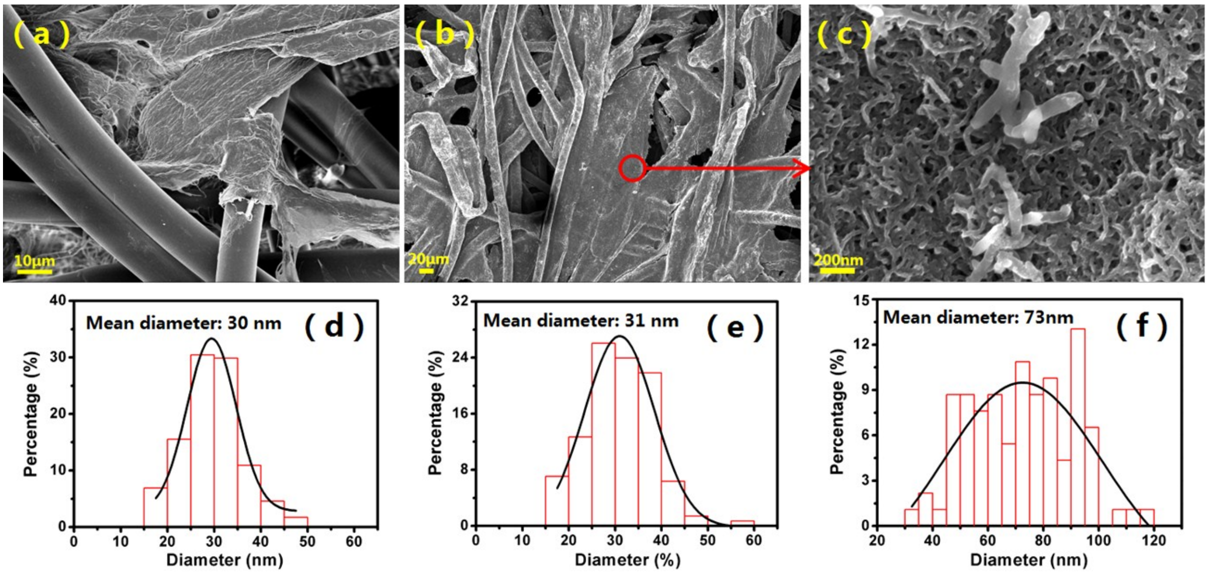

Fig. S2 SEM images of (a) original air-laid paper and (b)(c) A(2C0.7P)1 paper. Diameter distribution maps of PANI coated-CNTs in (d) A(2C0.1P)1 and (e) A(2C0.5P)*n* papers. (f) Diameter distribution map of PANI nano-fibers in A(2C0.5P)*n* papers.

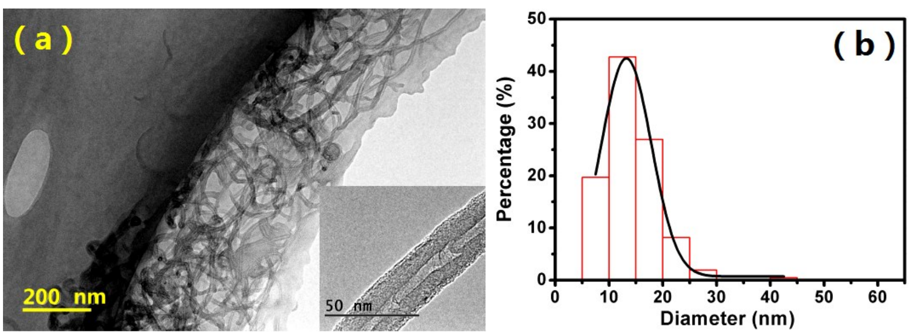

Fig. S3 (a) Transmission electron microscopy images of CNTs and (b) their diameter distribution map. The multi-walled CNTs have a mean diameter of ~14 nm.

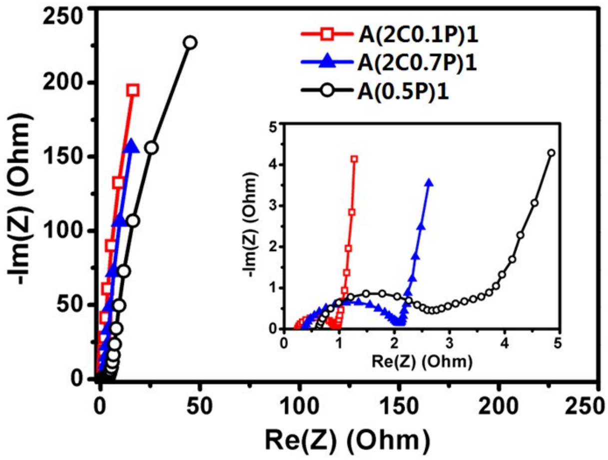

Fig. S4 Nyquist plots of A(2C0.1P)1, A(2C0.7P)1 and A(0.5P)1 paper electrodes based symmetric supercapacitors. For A(2C0.1P)1 and A(2C0.7P)1 electrodes, their nearly vertical lines in low frequency region suggest they have good capacitive behaviors. A(2C0.7P)1 shows a larger charge-transfer resistance compared with A(2C0.1P)1. Capacitive behavior of A(0.5P)1 paper electrode is not ideal and charge-transfer resistance is notably larger than that of A(2C0.1P)1 and A(2C0.7P)1.

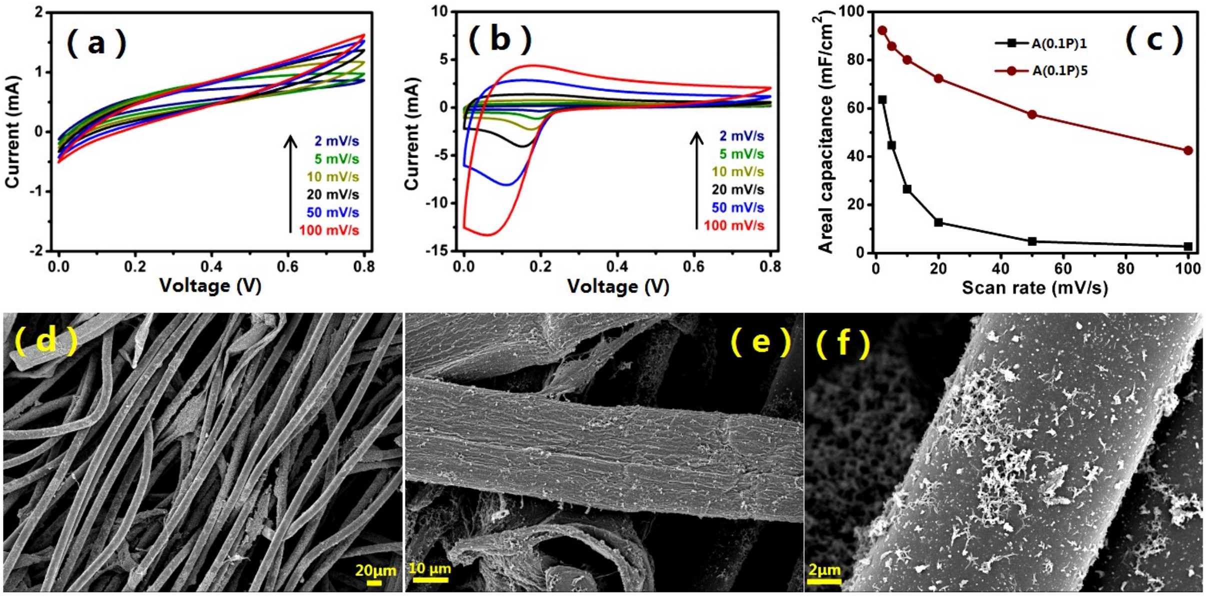

Fig. S5 CV curves of (a) A(0.1P)1 and (b) A(0.5P)1 paper electrodes based symmetric supercapacitors. (c) Areal capacitances of A(0.1P)1 and (b) A(0.5P)1 paper electrodes; (d)(e)(f) SEM images of A(0.5P)1 paper.

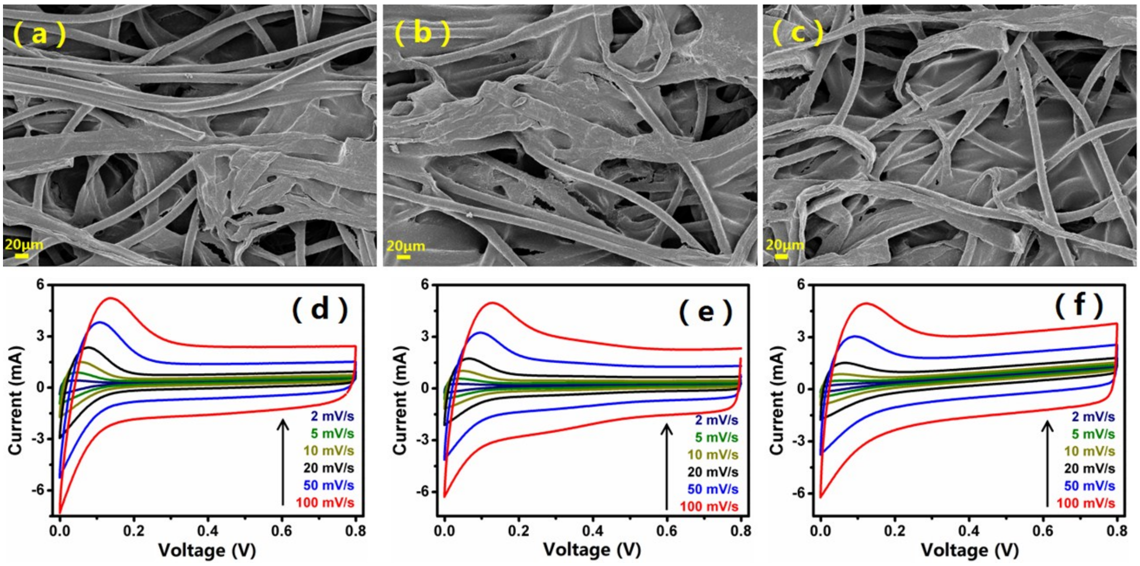

Fig. S6 SEM images of (a) A(2C)2, (b) A(2C)3 and (c) A(2C)4 papers. CV curves of (d) A(2C)2, (d) A(2C)3 and (e) A(2C)4 paper electrodes based symmetric supercapacitors.

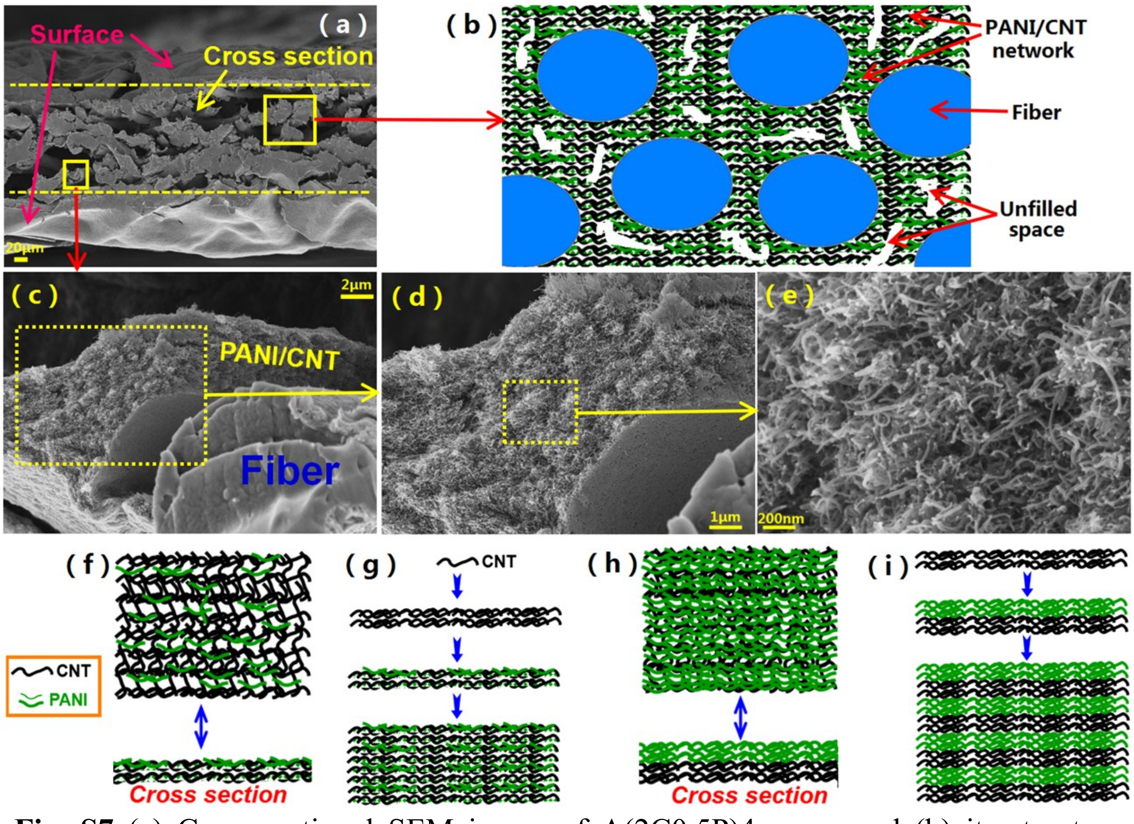

Fig. S7 (a) Cross-sectional SEM image of A(2C0.5P)4 paper and (b) its structure schematic (The "Fiber" means framework of paper substrate, *i.e.*, cellulose fibers and polyester fibers). (c)(d)(e) are magnified SEM images of PANI/CNT networks in (a). Structure schematics of PANI/CNT networks in (f) A(2C0.5P)1 and (g) A(2C0.5P)4 papers. (h)(i) Structure schematics of fictitious PANI/CNT networks with a laminated structure. We can see that polyester fibers and cellulose fibers serve as structural framework of air-laid paper substrate, while introduced PANI/CNT composite networks distribute in the space inside paper substrate (or can be regarded as distributing around the fibers). Obviously, the PANI/CNT networks are porous and have different thickness in different locations (but the whole paper electrode has a constant thickness of ~210 μm). The PANI/CNT networks do not possess a laminated structure in A(2C0.5P)4 paper electrode, even though they are introduced into paper substrates *via* a layer-by-layer deposition method. Potential reasons are as follows. (1) Fibrillar PANI nanoparticles scatteredly disperse on CNT network surface (Figure 3d in the main text) and do not form a dense PANI layer like that in (h) (of this figure). Therefore, when further deposit CNTs (and PANI), the CNTs and pre-deposited ones will mix together, instead of separating by PANI layer to form a CNT layer/PANI layer/CNT layer sandwich structure. Consequently, PANI/CNT network in A(2C0.5P)4 will not have a laminated structure (like that in (i) of this figure). (2) Fibrillar PANI nanoparticles have very similar morphologies with the deposited CNTs and other PANI tightly coats on CNT surface (Figure 3d in the main text). These make it relatively hard to distinguish PANI from CNTs in cross-sectional SEM images of A(2C0.5P)4 sample. Regardless of these, PANI is observed on top-most layer of CNT network A(2C0.5P)1, A(2C0.5P)2, A(2C0.5P)3 and A(2C0.5P)4, which suggests that PANI indeed exists on each layer of CNT network in A(2C0.5P)4, thus it is reasonable to use Figure 3e in the main text (*i.e.*, (g) in this figure) to depict micro-structure of PANI/CNT networks in A(2C0.5P)4 paper.

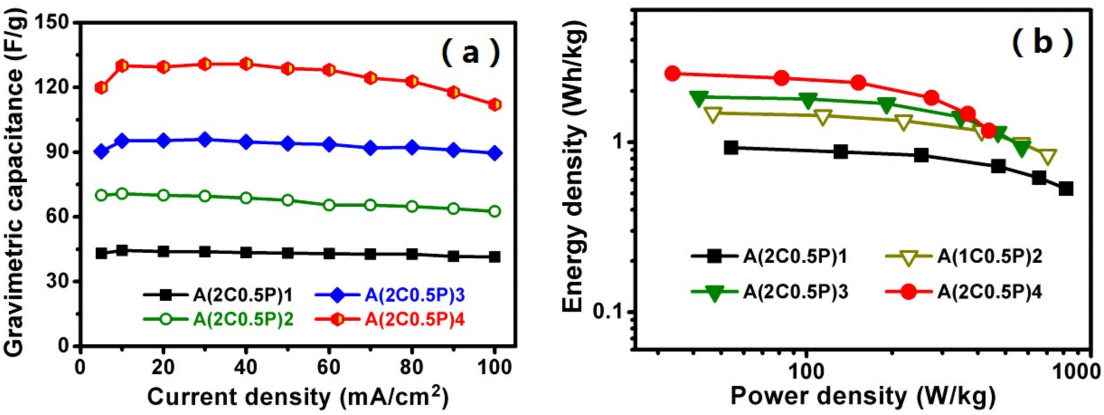

Fig. S8 (a) Gravimetric capacitance of A(2C0.5P)*n* paper electrodes and (b) mass specific energy density-powder density plots of paper electrode based symmetric supercapacitors.

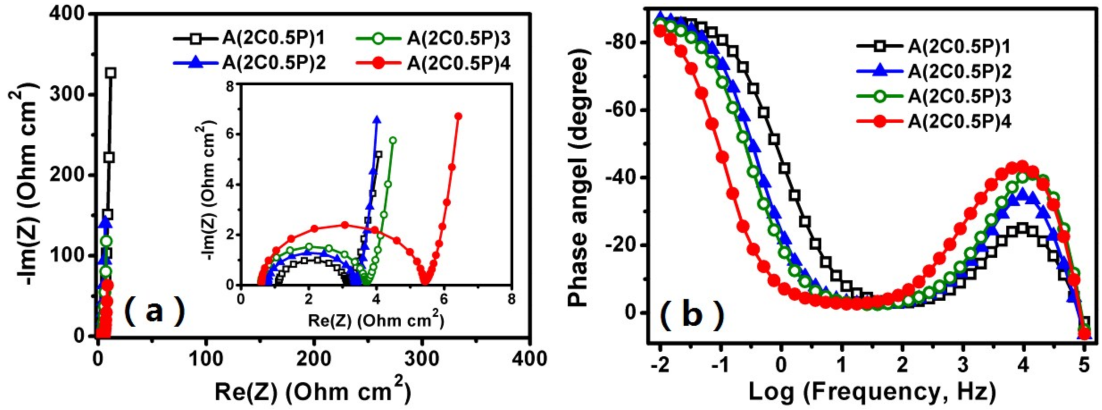

Fig. S9 (a) Fitted Nyquist plots (original Nyquist plots are given in Figure 5f in the main text) and (b) impedance phase angel *vs* frequency curves of A(2C0.5P)*n* paper electrodes based symmetric supercapacitors. Fitted value of charge-transfer resistance is 2.0, 2.6, 3.1 and 4.8 Ω cm^2, respectively, for A(2C0.5P)1, A(2C0.5P)2, A(2C0.5P)3 and A(2C0.5P)4. Capacitor response time ($1/f_0$, where f_0 is the frequency when impedance phase angel is -45^{o}) of A(2C0.5P)1, A(2C0.5P)2, A(2C0.5P)3 and A(2C0.5P)4 supercapacitors is calculated to be 1.0, 2.5, 3.3 and 9.0 s, respectively [S1,S2].

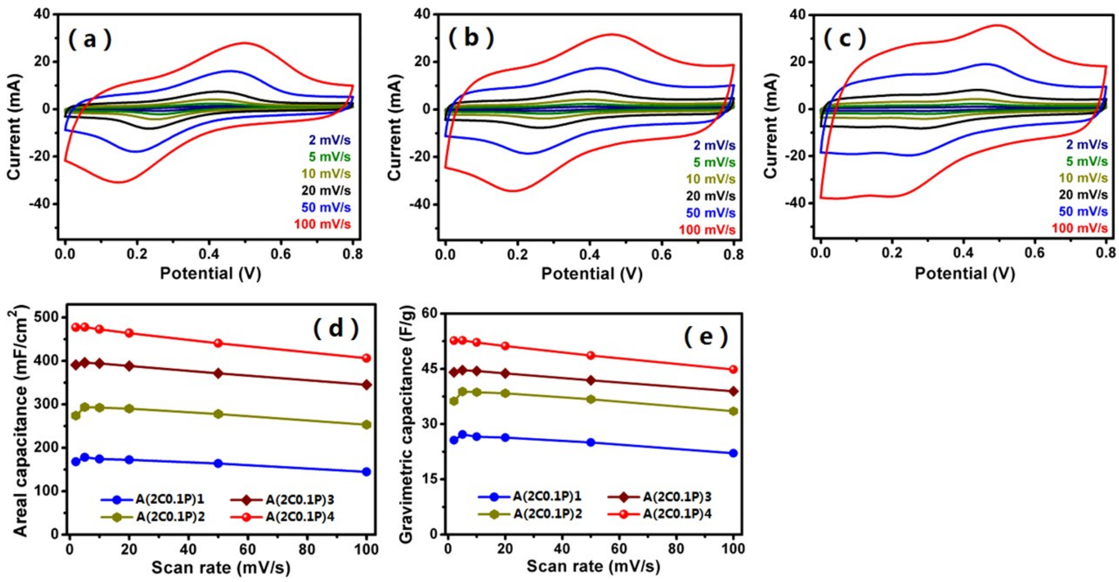

Fig. S10 CV curves of (a) A(2C0.1P)2, (b) A(2C0.1P)3 and (c) A(2C0.1P)4 paper electrodes based symmetric supercapacitors. (d) Areal capacitances and (e) gravimetric capacitance of A(2C0.1P)*n* paper electrodes.

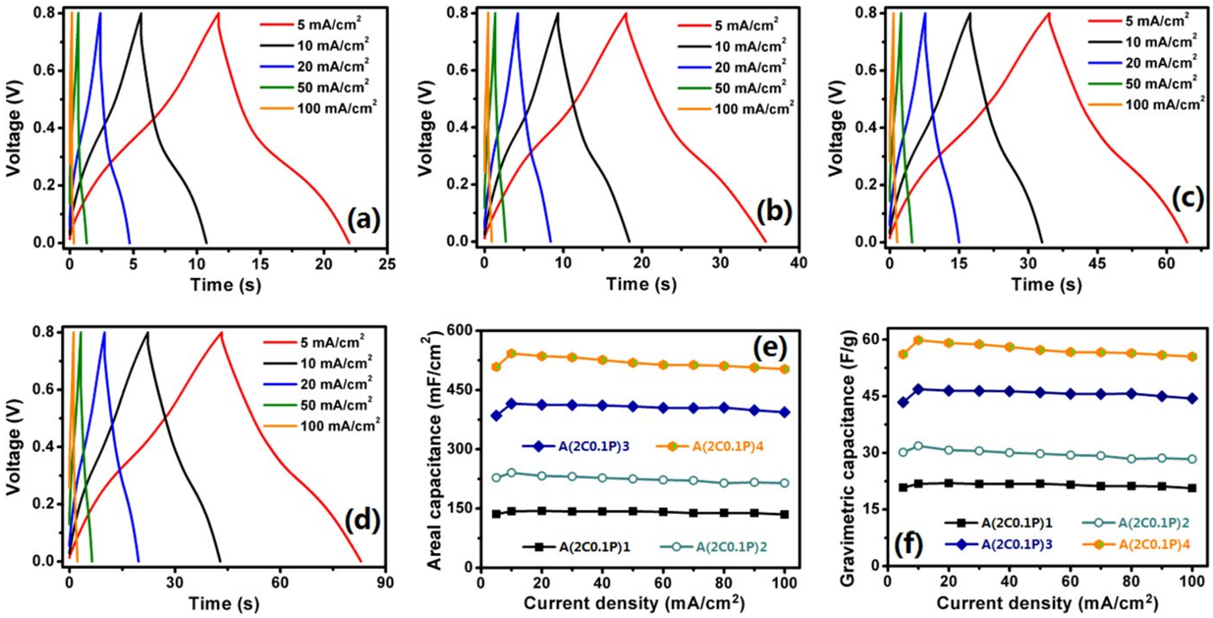

Fig. S11 GCD curves of (a) A(2C0.1P)1, (b) A(2C0.1P)2, (c) A(2C0.1P)3 and (d) A(2C0.1P)4 paper electrodes based symmetric supercapacitors. (e) Areal capacitances and (f) gravimetric capacitance of A(2C0.1P)*n* paper electrodes.

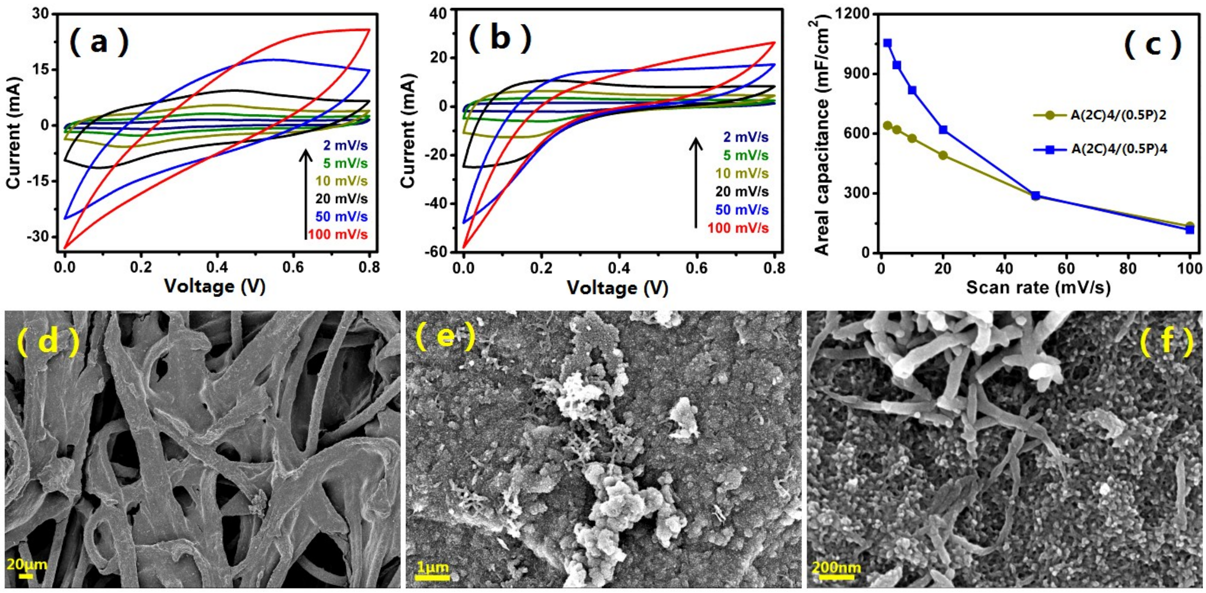

Fig. S12 PANI was repeatedly deposited on A(2C)4 paper for 2 and 4 times, and the obtained A(2C)4/PANI papers are noted as A(2C)4/(0.5P)2 and A(2C)4/(0.5P)4, respectively. CV curves of (a) A(2C)4/(0.5P)2 and (b) A(2C)4/(0.5P)4 paper electrodes based symmetric supercapacitors. (c) Areal capacitances of A(2C)4/(0.5P)2 and A(2C)4/(0.5P)4 paper electrodes. (d)(e)(f) SEM images of A(2C)4/(0.5P)4 paper (PANI loading in A(2C)4/(0.5P)4 is ~3.4 mg cm^{-2}).

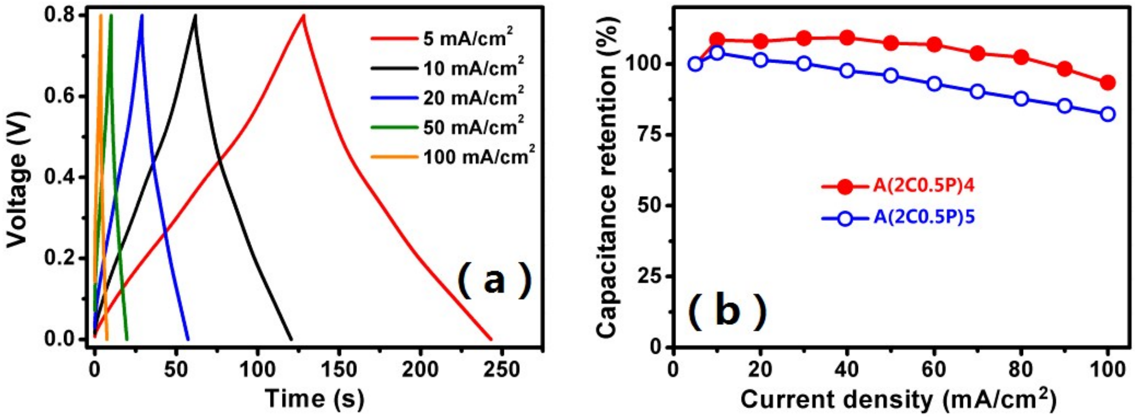

Fig. S13 (a) GCD curves of A(2C0.5P)5 paper electrode based symmetric supercapacitor. (b) Comparison of rate capability between A(2C0.5P)4 and A(2C0.5P)5 paper electrodes. At a low charge/discharge current of 5 mA cm^{-2}, areal capacitance of A(2C0.5P)5 is 6% higher than that of A(2C0.5P)4, but the former one's capacitance retention at large currents is notably lower than the latter one's, indicating a relatively poor rate capability.

Table S1 Electrochemical properties of flexible film-like electrodes reported in literature

Electrode	Loading of active materials	Areal capacitance [a]	Cycling performance	*Ref.*
PANI/CNT/paper	3.32 mg cm^{-2}	1506 mF cm^{-2} (10 mA cm^{-2}); 1298 mF cm^{-2} (100 mA cm^{-2})	82% after 11500 cycles	***This work***
Graphene/paper	0.675 mg cm^{-2}	81 mF cm^{-2} (1 mV s^{-1}); ~50 mF cm^{-2} (100 mV s^{-1})	~100% after 5000 cycles	S3
MnO_2/CNT/paper	CNT: 1.8 mg cm^{-2}; MnO_2: 0.1 mg cm^{-2}	123 mF cm^{-2} (1 mA cm^{-2})	97.8% after 20000 cycles	S4
PANI nanoribbon/single-walled CNT/paper	0.619 mg cm^{-2}	330 mF cm^{-2} (0.2 mA cm^{-2}); 248 mF cm^{-2} (2 mA cm^{-2})	79% after 1000 cycles	S5
Co_3O_4@MnO_2 array on stainless steel foil	1.5 mg cm^{-2}	560 mF cm^{-2} (11.25 mA cm^{-2})	97.3% after 5000 cycles	S6
Reduced graphene oxide (rGO)/MnO_2 film	3.7 mg cm^{-2}	802 mF cm^{-2} (0.1 A g^{-1}); <300 mF cm^{-2} (1 A g^{-1})	-	S7
rGO/Mn_3O_4 film	4.34 mg cm^{-2}	546 mF cm^{-2} (1 mV s^{-1}); ~195 mF cm^{-2} (50 mV s^{-1})	85% after 8000 cycles	S8
PANI/graphite/paper	-	356 mF cm^{-2} (0.5 mA cm^{-2}); ~240 mF cm^{-2} (5 mA cm^{-2})	83% after 10000 cycles	S9
MnO_2 on ITO-PET substrate	0.4 mg cm^{-2}	310 mF cm^{-2} (0.1 A g^{-1}); 190 mF cm^{-2} (1 A g^{-1})	-	S10
Polypyrrole/paper	1.85~3.54 mg cm^{-2}	1470 mF cm^{-2} (1 mA cm^{-2}); 640 mF cm^{-2} (20 mA cm^{-2})	75.6% after 10000 cycles	S11
VN nanowires/CNT film	-	178 mF cm^{-2} (1.1 mA cm^{-2}); 61 mF cm^{-2} (20 mA cm^{-2})	82% after 10000 cycles	S12
Graphene/CNT on PET substrate	-	2.54 mF cm^{-2} (10 mV s^{-1}) [b]	85% after 20000 cycles	S13
Polypyrrole/nanoporous gold film	11.48~179.1 μg cm^{-2}	1.8 mF cm^{-2} (100 mV s^{-1}) [b]	-	S14
Laser-scribed graphene film	36.3 μg cm^{-2}	3.67 mF cm^{-2} (1 A g^{-1}) [b]; 1.84 mF cm^{-2} (1000 A g^{-1}) [b]	96.5% after 10000 cycles	S15

[a] Some capacitance values listed in the table is read from data graphs in corresponding literature. There are some certain errors inevitably.
[b] The values are areal capacitances of supercapacitors.

References

[S1] W. Sugimoto, H. Iwata, K. Yokoshima, Y. Murakami, Y. Takasu, J Phys Chem B 2005, 109, 7330.

[S2] D. Yu, H. Wang, J. Yang, Z. Niu, H. Lu, Y. Yang, L. Cheng, L. Guo, ACS Appl Mater Interfaces 2017, doi: 10.1021/acsami.7b05318.

[S3] Z. Weng, Y. Su, D. W. Wang, F. Li, J. Du, H. M. Cheng, Adv Energy Mater 2011, 1, 917.

[S4] L. Dong, C. Xu, Y. Li, Z. Pan, G. Liang, E. Zhou, F. Kang, Q. H. Yang, Adv Mater 2016, 28, 9313.

[S5] D. Ge, L. Yang, L. Fan, C. Zhang, X. Xiao, Y. Gogotsi, S. Yang, Nano Energy 2015, 11, 568.

[S6] J. Liu, J. Jiang, C. Cheng, H. Li, J. Zhang, H. Gong, H. J. Fan, Adv Mater 2011, 23, 2076.

[S7] A. Sumboja, C. Y. Foo, X. Wang, P. S. Lee, Adv Mater 2013, 25, 2809.

[S8] Y. Hu, C. Guan, G. Feng, Q. Ke, X. Huang, J. Wang, Adv Funct Mater 2015, 25, 7291.

[S9] B. Yao, L. Yuan, X. Xiao, J. Zhang, Y. Qi, J. Zhou, J. Zhou, B. Hu, W. Chen, Nano Energy 2013, 2, 1071.

[S10] S. Shi, C. Xu, C. Yang, Y. Chen, J. Liu, F. Kang, Sci Rep 2013, 3, 2598.

[S11] L. Yuan, B. Yao, B. Hu, K. Huo, W. Chen, J. Zhou, Energy Environ Sci 2013, 6, 470.

[S12] X. Xiao, X. Peng, H. Jin, T. Li, C. Zhang, B. Gao, B. Hu, K. Huo, J. Zhou, Adv Mater 2013, 25, 5091.

[S13] J. Yun, D. Kim, G. Lee, J. S. Ha, Carbon 2014, 79, 156.

[S14] F. Meng, Y. Ding, Adv Mater 2011, 23, 4098.

[S15] M. F. El-Kady, V. Strong, S. Dubin, R. B. Kaner, Science 2012, 335, 1326.